MATHEMATICAL MODELING OF AN INDUCED DECREASE IN THE GRAGRAPHIC CLOUDS OPTICAL THICKNESS

M.F. Khairutdinov and V.I. Khvorost'yanov

Central Aerological Observatory, Dolgoprudnyi
Received November 27, 1989

We present the results of numerical simulation of the evolution of optical and microphysical characteristics of the lower level orographic clouds which are periodically seeded by dry ice in the course of airborne experiments to provide conditions necessary for astronomical observations. These characteristics are compared before and after cloudiness modification for different seeding regimes. Recommendations are given on the cloud dissipation technique to be used for minimizing the optical thickness of a cloud in a given range of observation angles.

Introduction. Orographic clouds observed in the atmosphere are formed under the impact of wave motions which appear due to air flow around the mountains and highlands.[1] Astronomical observatories and stations for remote sensing of the atmosphere are, as a rule, constructed on tops of mountain ridges to reduce the effect of atmospheric turbidity. However, orographic clouds may seriously hamper optical observations. At some critical moment of observations, e.g., during a solar eclipse meteorological conditions may suddenly appear unfavorable because of a cloud cover developed due to orographic ascent of air. For this reason there can arise a problem on artificial dispersal of such clouds.

Characteristic cloud cap formed just over the ridge is the main obstacle preventing optical observations. Because of an orographic ascent along the windward ridge slope the air mass is cooled, and, at once, as the process reaches saturation, condensation takes place, i.e., cloud droplets are being formed.

When the air mass descends along the leeward ridge slope, it is heated up and this results in its undersaturation, i.e., cloud droplets are starting to evaporate. Thus, the cloud cover above the mountain ridge is actually a current of cloud droplets which are continuously forming on the windward cloud boundary, and continuously evaporating on the leeward cloud boundary after being transferred over the ridge.[1]

Cloud droplets are approximately 10 μm in size. Naturally, such fine droplets at high number densities, strongly scatter sunlight, making optical observations impossible. Thus there arises a problem on dispersal of the cloud cap over the ridge. This can be made e.g., by of seeding the cloud from an aircraft with granulated dry ice.

Practical works on dispersal of the continuous stratiformis clouds have been undertaken in our country over large territories for different purposes, in particular, to provide favorable conditions for astronomical observations. In February, 1961 two-layer cloudiness was successfully dispersed over Crimea during the solar eclipse.[2] Artificial precipitation enhancement in mountain regions has also found wide use, including induced precipitations originating from orthographic clouds.[1,3] Mathematical models of the process precipitation initiation by seeding the orthographic clouds have also been developed.[4,5]

However, numerical calculations of artificial crystallization in a cloud over a mountain ridge aimed at decreasing the cloud optical thickness were not performed. Therefore a necessity has arisen to construct a mathematical model of artificial dispersal of orographic clouds, which would clarify principal trends of this process, as well as to formulate, practical on the basis of numerical simulation, some recommendations.

To modify the orographic clouds we have chosen a technique of periodically seeding such clouds with a coolant from an airborne. The periodical character of seeding is an essential feature of such a procedure since at continuous generation of cloud droplets on the windward side of the cloud cap.

In contrast to our earlier model[4,5] in which the speed of ascending air flow does not change with height, the present model includes a newly developed routine for computing the dynamics of air flow around the orographic obstacle, which accounts for the wind shear with height when modeling the cloud seeding by dry ice from an aircraft. This routine was tested when we computed zones of enhanced aerosol scattering within the internal gravity waves of mountainous regions.[6]

Model formulation. To compute the speed field we used a linear approximation of the analytical solution of the problem on describing the process of the mountain ridge streaming over by a vertically stratified air flow,[7] because in our case the tangent of the ridge slope angle does not exceed 1/25 and the values of perturbations of the meteorological elements φ' are much less that their values φ_0 in the stream $|\varphi'| \ll |\varphi_0|$.

0235-6880/90/07 701-08 $02.00

Let the x axis be directed air along the stream axis and the z axis be directed vertically. Below we represent a solution for the displacement of the stream lines from the level r for the ridge profile given by

$$h(x) = \frac{a^2 b}{a^2 + \left[x - x_0 \right]}, \tag{1}$$

where a is the ridge half-width, b is its height relative to its foot, and x_0 is the coordinate of the top. Then

$$\zeta(x, z) = \frac{U_0(0)}{U_0(z)} ab \exp\left\{ \frac{g - R\gamma}{2RT_0} z \right\} \times$$

$$\times \left[\frac{J_0\left(\beta e^{-\lambda z/2}\right)}{J_0(\beta) ab} h(x) - \pi\lambda\theta\left(x - x_0\right) \times \right.$$

$$\left. \times \sum_{n=1}^{N} \left[e^{-ak} \sin\left[k\left(x - x_0\right)\right] \frac{\sqrt{k^2 - \alpha_1}}{K} \times \right.\right.$$

$$\left.\left. \times \frac{J_\nu\left(\beta\, e^{-\lambda z/2}\right)}{\frac{d}{d\nu} J_\nu(\beta)} \right]_{k=k_n} \right]. \tag{2}$$

Here $U_0(z)$ and $T_0(z)$ are the background values of the horizontal speed and temperature, $\gamma = -\frac{dT_0}{dz}$, R is the gas constant for air, $g = 9.81$ m/s^2, $\beta = \frac{2\sqrt{\alpha_0}}{\lambda}$, $\nu = \frac{2}{\lambda}\sqrt{k^2 - \alpha_1}$, $J_0(x)$ and $J_\nu(x)$ are the Bessel functions of the first kind, K_n are the roots of the equation $J_\nu(\beta) = 0$, N is the number of root, $\theta(x)$ is the Heaviside function, and α_0, α_1 and λ are the auxiliary parameters characterizing the overflowing stream.[7]

The Cartesian components of the speed are expressed in terms of the displacement ξ as follows:

$$\omega_d = u_0(z) \frac{d\zeta}{dx} \left[1 - \left(\frac{d\zeta}{dx} \right)^2 \right]^{-1/2};$$

$$u_d = \sqrt{u_0^2(z) - \omega_d^2}. \tag{3}$$

For computer calculations of microphysical processes in the clouds it is convenient to transfer from Cartesian to a system of curvilinear coordinates

$$x' = x, \quad z' = z - h(x). \tag{4}$$

Then the kinetic equations for the droplet f_1 and crystal f_2 size distribution functions together with the equations for temperature T and humidity q take in the system of curvilinear coordinates the form (hereafter we shall omit primes)[4,5,8,9]

$$\frac{\partial T}{\partial t} + u \frac{\partial T}{\partial x} + \omega \frac{\partial T}{\partial z} = \frac{L_1}{C_p} \varepsilon_{c_1} + \frac{L_2}{C_p} \varepsilon_{c_2} + \frac{L_F}{C_p} \varepsilon_F -$$

$$- \gamma_a \omega_d + \Delta' T; \tag{5}$$

$$\frac{\partial q}{\partial t} + u \frac{\partial q}{\partial x} + \omega \frac{\partial q}{\partial z} = - \varepsilon_{c_1} - \varepsilon_{c_2} - \Delta' q; \tag{6}$$

$$\frac{\partial f_1}{\partial t} + u \frac{\partial f_1}{\partial x} + \left(\omega - v_1(r_1)\right) \frac{\partial f_1}{\partial z} + \frac{\partial}{\partial r_1} \dot{r}_1 f_1 =$$

$$= \left[\frac{\partial f_1}{\partial t} \right]_{col} + J_{1a} + J_1 + \Delta' f_1; \tag{7}$$

$$\frac{\partial f_2}{\partial t} + u \frac{\partial f_2}{\partial x} + \left(\omega - v_2(r_2)\right) \frac{\partial f_2}{\partial z} + \frac{\partial}{\partial r_2} \dot{r}_2 f_2 =$$

$$= \left[\frac{\partial f_2}{\partial t} \right]_{col} + J_2 + \Delta' f_2; \tag{8}$$

$$\dot{r}_i = \frac{D\Delta_i \rho_a k_f}{\rho_i r_i \Gamma_i \xi_i^2}; \qquad \Gamma_i = 1 + \frac{L_i}{C_p} \frac{\partial q_{si}}{\partial T};$$

$$\Delta' = \frac{\partial}{\partial x} k_x \frac{\partial}{\partial x} + \frac{\partial}{\partial z} k_z \frac{\partial}{\partial z}; \tag{9}$$

$$\varepsilon_{c_i} = 4\pi\rho_i \xi_i \int_0^\infty r_i^2 \dot{r}_i f_i \, dr_i;$$

$$\varepsilon_F = \frac{4}{3} \pi\rho_2 \xi_2 \int_0^\infty r_1^2 J_{1F}(r_1, T) \, dr_1, \tag{10}$$

where u and w are the horizontal and vertical speed components in the curvilinear coordinate system which are written in terms of their Cartesian counterparts u_d and w_d

$$u = u_d; \qquad \omega = \omega_d - u_d \frac{dh}{dx}. \tag{11}$$

Index $I = 1$ refers to droplets and $I = 2$ is used for crystals, k_x and k_z are the coefficients of horizontal and vertical turbulent diffusion, $\dot{r}_1$ is the rate of growth for an individual droplet or crystal, $v_1(r_1)$ is rate of the droplet fall, q_{si} are the values of saturating humidity over water or ice surface, $\Delta_I = q - q_{si}$ is the supersaturation, D is the coefficient of molecular vapor diffusion in air, ρ_a, ρ_1, and ρ_2 are air, water, and ice densities, respectively, k_f and ξ_1 are the shape

factor and the ratio of the particle characteristic sizes, ε_{c_1} are the condensation and sublimation rates for water vapor, ε_F is the rate of droplet freezing, Γ_1 is the psychrometric correction factor, L_1 is the heat of vaporization for droplets and crystals, L_F is the heat of freezing for droplets, C_p is the specific heat of air, $\left(\frac{df_1}{dt}\right)_{col}$ is the rate of change in droplet and crystal size spectra due to coagulation and accretion, J_1 and J_2 are functions describing droplet freezing and nucleation on natural sublimation nuclei, J_{1a} is the function describing the origin of new droplets on atmospheric condensation nuclei, and $\gamma_a = \frac{g}{C_p}$.

Expressions for droplet and crystal rates of fall were specified similarly.[8–10]

Expressions for J_1 and J_{1a} in the right side of Eqs. (8) and (9) were parameterized in the same way as in Refs. 8 and 11.

After computer calculations of the droplet f_1 and crystal f_g size distribution functions it is possible to define the following variables: the water content q_{L1}, the ice content q_{L2}, the droplet N_1 and crystal N_2 number densities, and their mean radii $\bar{r}_1$

$$q_{L_1} = \frac{4}{3}\pi\rho_1 \int_0^\infty r_1^3 f_1 \, dr_1; \tag{12}$$

$$N_1 = \int_0^\infty f_1 dr_1; \tag{13}$$

$$\bar{r}_1 = \frac{1}{N_1}\int_0^\infty r_1 f_1 \, dr_1; \tag{14}$$

Using optical characteristics it is also possible to calculate scattering cross section per unit of a cloud as well as the cloud optical thickness τ along a chosen direction l (Refs. 12 and 13)

$$\sigma = 2\pi \left[\int_0^\infty r_1^2 f_1 dr_1 + 2 \left[\int_0^\infty r_2^2 f_2 dr_2 \right] \times \right.$$

$$\left. \times \left[\frac{2.5}{\bar{r}_2} \left[\frac{6q_{L2}}{\pi\rho_2 N_2} \right]^{1/3} - 3 \right]^{-1} \right]; \tag{15}$$

$$\tau_1 = \int_0^1 \sigma \, dl. \tag{16}$$

From the value of optical thickness τ_1 one can determine the cloud transmission from the relation $I = I_0 \cdot e\tau_1$.

Airborne seeding was modeled by introducing crystals with the size r_c and the number density P_{cr}[dm^{-3}] at the nodes of the finite difference grid along the whole seeding track. The agent consumption per one kilometer of a plane route was found from the formula

$$Q = \frac{P_{cr}\,\Delta x\,\Delta z_s}{N_{CO_2}} \cdot 10^9, \tag{17}$$

where Δx is the grid step along the x axis, in km, Δz_s is the thickness of seeding, in km, $N_{CO_2} = 10^{12}$ is the number of crystals generated in the process of evaporation of 1 g of solid CO_2. The dimension of Q is in kg/km. The periodicity of seeding was simulated by repetition of this "seeding" routine every 10 minutes of physical time. It corresponds to periodic airborne seeding when a plane is flying "figure eight" routes.

The initial stage in numerical solution of the system of equations included calculating from Eqs. (2) and (3) the Cartesian components of the flow speed for prescribed profiles of $U_0(z)$ and $T_0(z)$, when the model ridge described by Eq. (1) was overflowed. The next stage of calculating consisted in integrating the equations of microphysics. To this end a finite difference grid was introduced with the 31 by 41 dimensionality along the vertical and horizontal directions at constant increments Δz and Δx, respectively.

While solving the equations of thermohydrodynamics and microphysics we employed the so-called splitting technique, developed by G.I. Marchuk et al.[14] The first stage of this technique accounts for horizontal transfer, the second — for the vertical transfer, and the third — for the processes of condensation, sublimation, and water vapor distillation from droplets to crystals. Finally, at the fourth stage the processes of coagulation and accretion were calculated. This technique is described in detail in Refs. 8, 9, and 13.

After computer calculations of the components of speed in the curvilinear coordinate system according to Eq. (11) we prescribed the initial fields of T, q, and f_1 as follows. At the initial moment $f_1(x, z, r_1, t) = 0$ at all nodes of the grid. The fields of T and q were assumed to be homogeneous along the curvilinear coordinate x'. The temperature profile was in the form $T_0(z) = T_0(0) - \gamma z$, and the profile of relative humidity was described by the exponential law

$$q_r(z) = q_{r_0} \exp\left(-z/A_D\right), \tag{18}$$

which, on the average, describes quite well the behavior of tropospheric T and q.

Numerical results. ~ The differential grid calculations covered 40 km along the x axis, with the step of 1 km, and 3 km along the z axis with the step of 0.1 km. The ridge height was $b = 0.6$, its half-width was $a = 10$, and $x_0 = 20$ km. To study the vertical wind shear effect upon crystallization zone the wind velocity profile U_0 [m/s] was given in the form:

$U_0(z) = 5 + 1.43z$, where z was in km. In addition, the following set of parameters was used $\gamma = -\frac{dT_c}{dT} = 6°C \cdot m^{-1}$, $T_0(0) = -5°C$, $k_x = 50\ m^2 \cdot s^{-1}$, $k_z = 5\ m^2 \cdot s^{-1}$, $A_D = 8$ km, $q_{r0} = 90\%$, and $r_c = 20$ μm. The time step $\Delta t = 60$ s was taken.

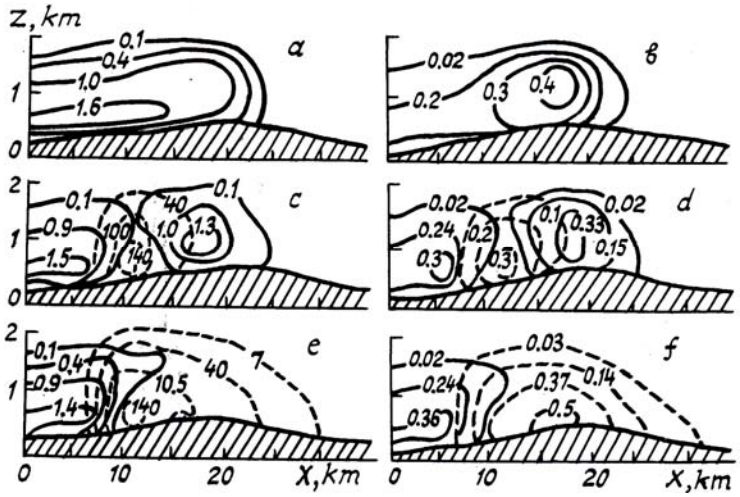

FIG. 1. Isolines of particle concentration for droplets $N_1 \cdot 10^5\ g^{-1}$ *(solid curves) and crystals* N_2, g^{-1} *(dashed curves) (a, c, and e); the fields of liquid water content* q_{L1}, *in* g/kg *(solid curves) and the ice content* q_{L2} *in* g/kg *(dashed curves) (b, d, and f); before seeding starts (a, b);* 20 min *after seeding starts (c, d);* 50 min *after seeding starts (c, f).*

TABLE I.

Variant No	Seeding track distance, km	P_{cr}, dm^{-3}	Agent consumption, Q, kg/km	Seeding track top, km	Seeding track bottom, km	Vertical optical thickness over the ridge top
1	13	500	0.9	2.0	0.2	4.0
2	13	200	0.4	2.0	0.5	9.5
3	13	2000	1.4	1.7	1.0	8
4	16	500	0.75	2.0	0.5	3
5	16	1500	2.25	2.0	0.5	7.5
6	16	3000	4.5	1.7	0.2	12
7	8	500	0.75	1.7	0.2	5.5
8	5	1500	2.25	1.7	0.2	11.5

Figures 1a and b present the water content and droplet number density fields in the cloud, 1.5 hours after its natural evolution. Cloud water content amounts to 0.4 g/kg. The crystal phase is practically absent, despite considerable supersaturation above the ice surface (20%). This fact results from the low value of probability of droplet freezing ($J_1 \sim r^3$), since during the relatively short time when the takes droplet is being transferred through the cloud, droplet can not grow to a sufficiently large size. In addition, the temperature in the region occupied by the cloud does not drop below −25°C, this fact also explains the decrease of the cloud droplet freezing efficiency ($J_1 \sim \exp(273 - T)$). At such temperatures sublimation nuclei remain practically inactive. Water droplets generated at the left cloud boundary are pumped through the cloud and then entrapped by the descending air flow beyond the ridge top they dissipate.

The table shows for various seeding regimes the values of vertical optical thickness of a cloud above the ridge top, this value is a quantitative characteristic of the atmospheric noise in optical observations. In the course of numerical experiments seeding track distance from the ridge top and agent consumption were varied. The seeding thickness varied only insignificantly. Seeding periodicity of 10 minutes was chosen which is close to an actually possible regime, if only one airplane is used. The process of cloud droplet crystallization is clearly illustrated by Figs, 1a–f (regime 1). In this regime the seeding track was plotted at a

distance of 13 km from the ridge top. The agent consumption was 0.9 kg per one kilometer of the track along the ridge, so that seeding covers practically the entire cloud thickness. In twenty minutes after seeding starts, a typical "dip" appeared in the water- droplet phase (Fig. 1c and d), at a distance of approximately 5 km downwind from the seeding track. Ice content amounted to 0.3 g/kg in the center of the crystallization zone. This zone of crystallization was vertically inhomogeneous and inclined leeward that is caused by the effect of the wind shear. Indeed, due to higher rate of transfer the artificial crystals located at the top of the cloud traveled longer distances than the crystals at the cloud bottom. Due to the high supersaturation above ice, the crystals quickly "grow" consuming the liquid phase and fall down precipitating at the ridge slopes as snow. Fifty minutes after the periodic seeding started the cloud to the right of the seeding track was completely crystallized (Fig. 1e and f).

The main points of the dispersal are illustrated by Fig. 2. Before seeding starts the cloud was formed exclusively by the liquid droplets with the mean radius ~8 μm and the droplet number density to $1.4 \cdot 10^5$ g^{-1}, and liquid water content up to 38 g/kg. in a cloud base. Over the ridge the optical thickness of such a cloud was 64.

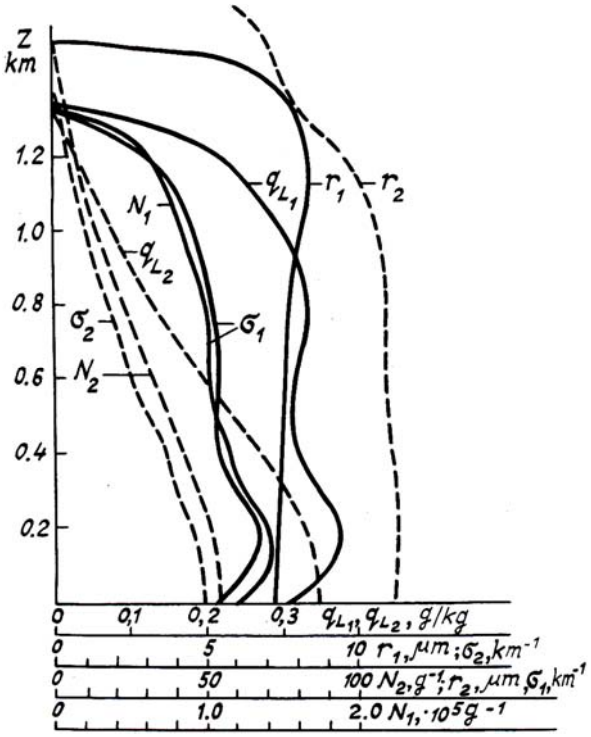

FIG. 2. Vertical cross section of the cloud cap over the ridge top before (solid curves) and during seeding (dashed curves) for regime 4; N_1 and N_2 are the droplet and crystal number density, respectively; $\bar{r}_1$ and $\bar{r}_2$ are their mean radii; q_{L1} and q_{L2} are the liquid water content and ice content; σ_1 and σ_2 are the light scattering cross sections.

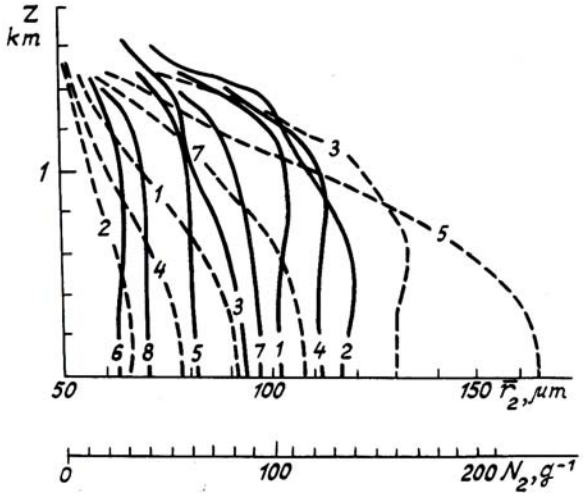

FIG. 3. Vertical cross section of the cloud cap over the ridge top for different seeding regimes (see the table); solid lines stands for the mean crystal radii $\bar{r}_2$; dashed lines stands for the crystal number density N_2.

It is interesting to note that the profile of the scattering cross section σ_1 virtually follows the profiles of N_1 and q_{L1}. After seeding, the cloud above the ridge top was entirely composed of crystals with the mean radius of crystals ~ 120 μm, crystal number density up to 55 g^{-1} at the cloud base, and ice content up to 0.35 g/kg. It should be noted that the profile σ_2 also follows the profile of N_2. So one can assume that the scattering cross-section profile is mainly determined by the profile of particle number density. The lowest value of the vertical optical cloud thickness $\tau = 3$ was obtained for regime 4; this thickness appears to be sufficiently low for observing such an event as the solar eclipse. Figure 3 presents the profiles of the mean crystal radii (solid lines) and their number density (dashed lines) for various regimes of seeding above the ridge top. So we may take the fourth regime as the basic and compare all other regimes with it.

Let us now study first the regime 5. It follows from Fig. 3 that In comparison with regime 4 overseeding took place during regime 5; the mean crystal radius in that case was 30 μm less than in the basic regime, although in both cases the seeding track was at the same distance from the ridge. Owing to this fact, the rate with witch such crystals fall out was less and time is not enough for crystals to fall out from the cloud and reach the ridge top. For this reason the optical thickness was 7.5 for regime 5. The same can be said relative to regime 6, for which we have $\tau = 12$. Forthcoming the seeding track to the ridge top deteriorates the result. Let us study, for example, regime 1. The seeding track forthcoming to the ridge top results in the higher number density of crystals than for regime 4, though the consumption of the agent was practically identical to that in the regime 4. This fact results in τ increase up to 4.

Reduction of the agent consumption does not yield better results, as illustrated by regime 2. It follows from Fig. 3 that in the regime 2 the crystal number density become lower as compared to that in the regime 4, however the optical thickness is $\tau = 9.5$. This result is explained as follows: in regime 2 the seeded cloud is not crystallized completely, and many droplets remain over the ridge top. In other words, complete pumping of water vapor from droplets to crystals fails because of low number density of crystals introduced into the cloud. Thus the rigorously determined dose of agent exists for each given cloud and fixed given distance from the seeding track to ridge top, which produces the maximum clearing-up effect. Regimes 7 and 8 demonstrate the effect of seeding track forthcoming to the ridge top. As one can expect, in this case, a negative dispersal effect is observed. The fact is that the short transfer time to the ridge top prevents the crystals from complete precipitating at the windward slope.

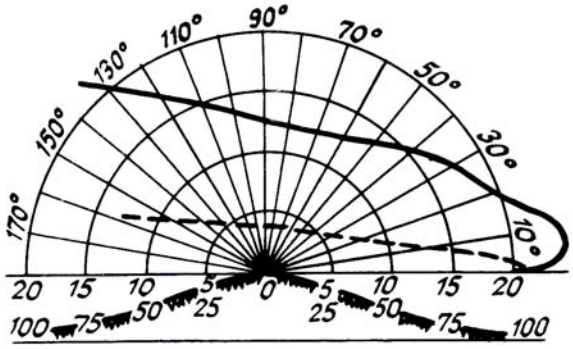

FIG. 4. Angular distribution of the cloud optical thickness τ, relative to ridge top in the polar coordinate system prior to (solid curve), and after seeding (dashed curve), (regime 4); the radial axis shows the values of τ prior to (lower scale) and after seeding (upper scale); the angular scale shows observation angles relative to the horizon.

Along with modification of the vertical optical thickness for different seeding regimes we also investigated its angular distribution with respect to the ridge top. Let us assume that an optical system is positioned at the top, which is capable of sensing the atmosphere in a scanning mode. Starting from a known distribution of scattering cross section it is possible then to obtain the angular distribution of the cloud optical thickness, and to use it for selecting the optimal observation angle. We based our estimates on most effective regime 4. The angular distribution of τ in the cloud is presented in Fig. 4. The solid line corresponds to cloud state before seeding and the dashed line corresponds to the regime of periodic seeding (regime 4). Both curves are plotted in the polar coordinate system with the cloud optical thickness shown along the radial axis before seeding (lower scale) and after it (upper scale). Observation angles counted from the horizon are plotted along the angular scale. For example, the optical thickness of the cloud before seeding was equal to 80 at an angle of 40° to the horizon and decreased to 5 after seeding. Now let an optical instrument designed to observe certain light source, e.g., the sun during its eclipse, be sensitive to the solar light only if its intensity is not attenuated by more that 100 times, i.e., the cloud optical thickness does not exceed 4.6. Then it is evident from the lower curve in Fig. 4 that observation will be successful if the sun remains in the angular sector between 50 and 120° relative to the horizon. In all the other cases observation will be strongly hampered. It is interesting to note that the lowest optical thickness is observed at an angle about 80°, and not along the vertical direction, i.e., the direction of highest transparency in a seeded cloud is inclined windward.

CONCLUSIONS

Now we draw the principal conclusions and recommendations retrieved from numerical simulations of the artificial crystallization of a cloud aimed at its dispersal.

a) On the one hand, the seeding track must be rather far from the ridge top so that the precipitation particles generated in the cloud succeed to fall out from onto the windward slope of the ridge, and on the other hand, it should be not too far from the ridge top so that to avoid the regeneration of the droplet phase due to the orographic ascent.

b) There exists an optimal dose of the agent for the chosen distance between the seeding track and the ridge; both over- and underseeding adversely affects the final result of seeding.

c) In the case of a positive effect of seeding there exists a rather narrow angular sector (several tens of degrees wide) of rather low optical thickness; the direction of highest transparency is inclined in the leeward direction.

d) Maintenance of the transparency window in quasistationary state would call for periodic seeding; a singular seeding episode would only provide a short-time effect because of the quick regeneration of the droplet phase.

In conclusion the authors would like to acknowledge G.R. Toroyan for his valuable comments and discussions in the course of this work.

REFERENCES

1. A. Dennis, *Weather Modification by Cloud Seeckng* [Russian translation] (Mir, Moscow, 1983).
2. E.K. Fedorov, Vestn. Akad. Nauk SSSR, No. 9. (1962).
3. Yu.S. Sedunov, Meteor. Gidrolog., No. 9, 5–17(1986).
4. K.Ya. Kondrat'yev, G.R. Toroyan, and V.I. Khvorost'yanov, Issled. Zemli iz Kosmosa, No. 1, 3–15 (1988).

5. G.R. Toroyan and V.I. Khvorost'yanov, Proc. Central Aerological Observatory, No. 164, 66–72 (1987).
6. K.Ya. Kondrat'ev, V.I. Khvorost'yanov, M.F. Khairutdinov, and S.Yu. Kudryavtsev, Atm. Opt., to be published (1990).
7. M.V. Buikov and A.M. Pirnach, Izv. Akad. Nauk SSSR, Ser. Fiz. Atm. Okeana **11**, No. 5, 469–480 (1975).
8. E.L. Kogan, I.P. Mazin, B.N. Sergeev, and V.I. Khvorost'yanov, *Numerical Simulation of Clouds* (Gidrometeoizdat, Moscow, 1984).
9. B.Dzh. Meison, *Cloud Physics*, [Russian translation) (Gidrometeoizdat, Moscow, 1961).
10. G.I. Marchuk, K.Ya. Kondrat'yev, V.V. Kozoderov, and V.I. Khvorost'yanov, *Clouds and Climate* [in Russian] (Gidrometeoizdat, Leningrad, 1986).
11. T. Ohtake and P.J. Huffman, J. Appl. Meteorol. **8**, No. 4 (1969).
12. V.I. Khvorost'yanov, Meteor. Gidrolog., No. 4 29–37 (1987).
13. G.I Marchuk, *Methods of Computational Mathematics* (Nauka, Moscow, 1973).